Applied Surface Science 258 (2012) 6643–6647

Contents lists available at SciVerse ScienceDirect

Applied Surface Science

journal homepage: www.elsevier.com/locate/apsusc

High performance ethanol sensing films fabricated from ZnO and In_2O_3 nanofibers with a double-layer structure

Xiao-Juan Zhang[a,b], Guan-Jun Qiao[a,*]

[a] State Key Laboratory for Mechanical Behavior of Materials, Xi'an Jiaotong University, Xi'an 710049, PR China
[b] School of Science, Xi'an Polytechnic University, Xi'an 710048, PR China

ARTICLE INFO

Article history:
Received 27 June 2011
Received in revised form 16 March 2012
Accepted 19 March 2012
Available online 28 March 2012

Keywords:
Semiconductors
Sensitivity
Sensing films
Gas sensors
Chemical sensors

ABSTRACT

ZnO and In_2O_3 nanofibers are synthesized via electrospinning methods, and characterized by X-ray diffraction (XRD), scanning electron microscopy (SEM), transmission electron microscope (TEM), infrared (IR) spectroscopy, and X-ray photoelectron spectroscopy (XPS). The nanofibers are deposited on ceramic substrates to form sensing films with various structures (ZnO nanofiber films, ZnO–In_2O_3 nanofiber films, and ZnO–In_2O_3–ZnO nanofiber films), and their sensing properties are investigated at different temperatures. Compared with ZnO nanofiber films and ZnO–In_2O_3–ZnO nanofiber films, the obtained ZnO–In_2O_3 nanofiber films exhibit improved and excellent sensing properties to ethanol. The highest sensitivity (the ratio of sensor resistance in air to that in target ambience) of 25 is obtained when the ZnO–In_2O_3 films are exposed to 100 ppm ethanol at 210 °C, while the corresponding values are only 8 for ZnO nanofiber films at 300 °C and 17 for ZnO–In_2O_3–ZnO nanofiber films at 210 °C. Rapid sensing reactions are also obtained as the response and recovery times of ZnO–In_2O_3 nanofiber films to 100 ppm ethanol are only about 2 and 1 s, respectively. These high sensing performances are explained by referring the heterocontacts formed by the double-layer structure.

1. Introduction

With a growing demand for environment monitoring, chemical gas sensors are attracting increasing interest due to the advantages of simple design, low weight and cost, and easy fabrication [1–4]. Metal-oxide semiconductor (MOS) materials (such as ZnO, In_2O_3, TiO_2, and SnO_2) are widely employed as the sensing materials in chemical sensors, and their gas sensing properties have been investigated for more than four decades [5–7]. Traditional MOS sensing materials are nanopowders, which commonly suffer from low sensitivity and long response time [8,9]. Scientists usually employ metal dopant to improve their performance [10], but the struggle often fails due to the aggregation growth among the nanopowders [11]. In this decade, researchers discover that reforming MOS at nanometer level can effectually improve their sensing properties [12–14]. In particular, one-dimensional (1D) nanostructure has been strongly proposed to be an effective platform for the preparation of gas sensing materials because they can make it easy and fast to translate the gas recognition into an electrical signal and then transport electron effectively [15,16]. Taking the advantages of small size, high density of surface sites and increased surface-to-volume ratios, many types of gas sensors based on 1D nanostructure MOS have been fabricated.

Both ZnO and In_2O_3 are typical functional MOS, which have been chosen as basic materials for chemical sensors, photodiodes, ultraviolet lasers, and solar cells [17,18]. For gas sensors, these two materials have been proved to own high sensitivity for the detection of both reducing (e.g., CO, CH_4, and H_2) and oxidizing gases (e.g., NO_X and O_2) [18]. Hitherto, many ZnO or In_2O_3 based 1D nanostructures with various performances have been reported [12]. However, most of them are obtained by doping noble or rare metals such as Pt and La in them to improve their sensing performance [17]. The high-performance sensing films based on double-layer structures have rarely been concerned.

Herein, we present a simple method to fabricate double-layer structure ZnO–In_2O_3 films via electrospinning. Electrospinning is a versatile and cost-efficient technique for producing multi-functional nanofibers from various polymers, polymer blends, composites, sol–gels, ceramics, etc. [19]. Electrospun nanofibers/nanowebs have remarkable characteristics such as large surface-to-volume ratio and with pore sizes in the nano range. The as-fabricated ZnO–In_2O_3 films exhibit low operating temperature, high sensitivity, and quick response and recovery to ethanol, which indicates the potential applications for ZnO–In_2O_3 films in gas sensors. Besides, the results also show that the double-layer film structure is greatly a benefit for the sensor performance,

* Corresponding author. Tel.: +86 29 83245275; fax: +86 29 83245275.
E-mail address: guanjunqiao@hotmail.com (G.-J. Qiao).

0169-4332/$ – see front matter © 2012 Elsevier B.V. All rights reserved.
doi:10.1016/j.apsusc.2012.03.098

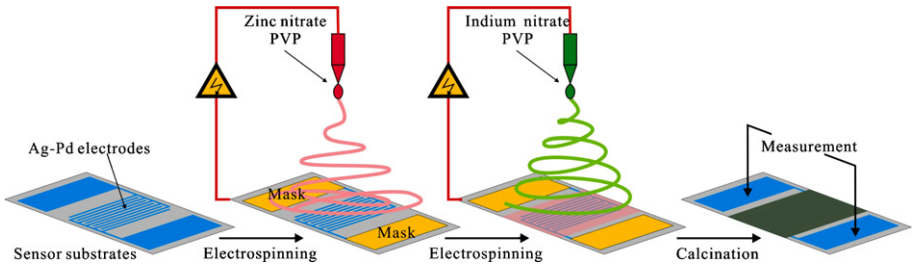

Fig. 1. Schematic diagram of the processing steps used to fabricate and measure ZnO–In_2O_3 nanofiber films.

thus may provide a possible route for sensing improvement of 1D nanostructure-based gas sensors.

2. Experimental

All chemicals (analytical grade reagents) were purchased from Shanghai Chem-reagent Group (China) and used as received without further purification. Sensor substrates were purchased from Beijing Elite Tech Co., Ltd. The electrospinning process in the present experiment is similar to those described previously for nanofiber synthesis [20,21]. In a typical procedure for ZnO precursory nanofibers, 0.60 g of zinc nitrate was added into 8.5 g of N, N-dimethylformamide (DMF) in a glove box under vigorous stirring for 6 h. Subsequently, 1 g of poly (vinyl pyrrolidone) (PVP, Mw = 1,300,000) was dissolved into 8 mL ethanol in another glove box under vigorous stirring for 6 h. Then, both of them was mixed together under stirring and then loaded into a glass syringe for electrospinning by applying a high voltage of 18 kV between the cathode (an aluminum foil) and anode (syringe) at a distance of 20 cm. The precursory nanofibers were collected on an aluminum foil. The sensor substrates (13.5 mm × 7 mm, 0.5 mm in thickness) with plastic masks (to cover the electrode-pin) were placed on the aluminum foil. There were five pairs of Ag-Pd interdigitated electrodes (both the width and distance were 200 μm) on the sensor substrate, and the electrodes could be calcined at 900 °C without any resistivity change. After electrospinning for 4 h, the sensor substrates were removed for the depositing of In_2O_3 precursory nanofibers. In this step, 0.38 g of indium nitrate was added to 8.8 g mixed solvent contained DMF/ethanol with the weight ratio of 1:1 and stirred for 2 h, and then 0.8 g of PVP was added to the above solution with stirring for 6 h. The obtained solution was then loaded into a glass syringe for electrospinning by applying a high voltage of 20 kV between the cathode (an aluminum foil) and anode (syringe) at a distance of 20 cm. After electrospinning for another 4 h, the sensor substrates were calcined at 600 °C in air for 5 h to convert the precursors into crystalline ZnO and In_2O_3 nanofibers. The obtained samples were designated as ZnO–In_2O_3 nanofiber sensors, and the fabricating process is illustrated in Fig. 1.

Two other type of samples were also fabricated for comparison, which were deposited ZnO nanofibers only (designated as ZnO nanofiber sensors) and deposited two times of ZnO nanofibers and one time of In_2O_3 nanofibers (designated as ZnO–In_2O_3–ZnO nanofiber sensors). A top view of sensor substrates, ZnO nanofiber sensors, ZnO–In_2O_3 nanofiber sensors, and ZnO–In_2O_3–ZnO nanofiber sensors are shown in Fig. 2(a).

Sensor measurement was performed on a CGS-1TP (Chemical gas sensor-1 temperature pressure) intelligent gas sensing analysis system (Beijing Elite Tech Co., Ltd, China). The analysis system offered an external temperature control (from room temperature to 500 °C), which could conductively adjust the sensor temperature with a precision of 1 °C. The sensors were laid on the temperature control and pre-heated at different operating temperatures for about 30 min. Two probes were pressed on sensor electrodes by controlling the position adjustment in the analysis system. When the resistance of the sensor was stable, saturated target gas was injected into the test chamber (18 L in volume) by a micro-injector through a rubber plug. The saturated target gas was mixed with air (relative humidity was about 25%) by two fans. After the sensor resistance reached a new constant value, the test chamber was opened to recover the sensors in air. The sensor resistance and sensitivity were collected and analyzed by the system in real time (Fig. 2(b)).

The sensitivity value (S) was designated as S = Ra/Rg, where Ra was the sensor resistance in air (base resistance) and Rg was a mixture of target gas and air. The time taken by the sensor resistance to change from Ra to Ra −90% × (Ra–Rg) was defined as response time when the target gas was introduced to the sensor, and the time taken from Rg to Rg +90% × (Ra–Rg) was defined as recovery time when the ambience was replaced by air.

X-ray powder diffraction (XRD) data were collected on an X'Pert MPD Philips diffractometer (Cu Kα X-radiation at 40 kV and 50 mA). Scanning electron microscopy (SEM) images were recorded on a SHIMADZU SSX-550 (Japan) instrument. Transmission electron microscope (TEM) images were obtained on a JEOL JEM-2000EX microscope with an accelerating voltage of 200 kV. Infrared (IR) spectroscopy was performed on a Bruker VERTEX 80 v/S infrared spectrometer in the range of 400–4000 cm^{-1} using KBr pellets

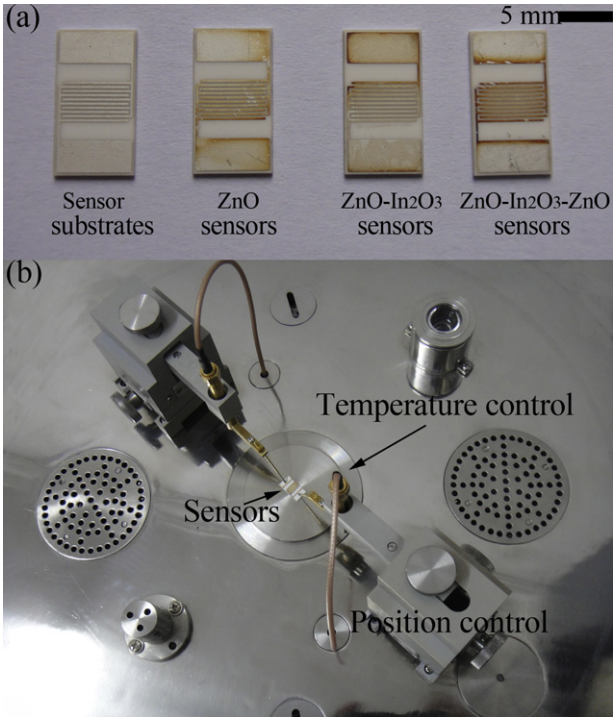

Fig. 2. (a) A top view of sensor substrates and sample sensors, and (b) a photograph of the gas sensing analysis system.

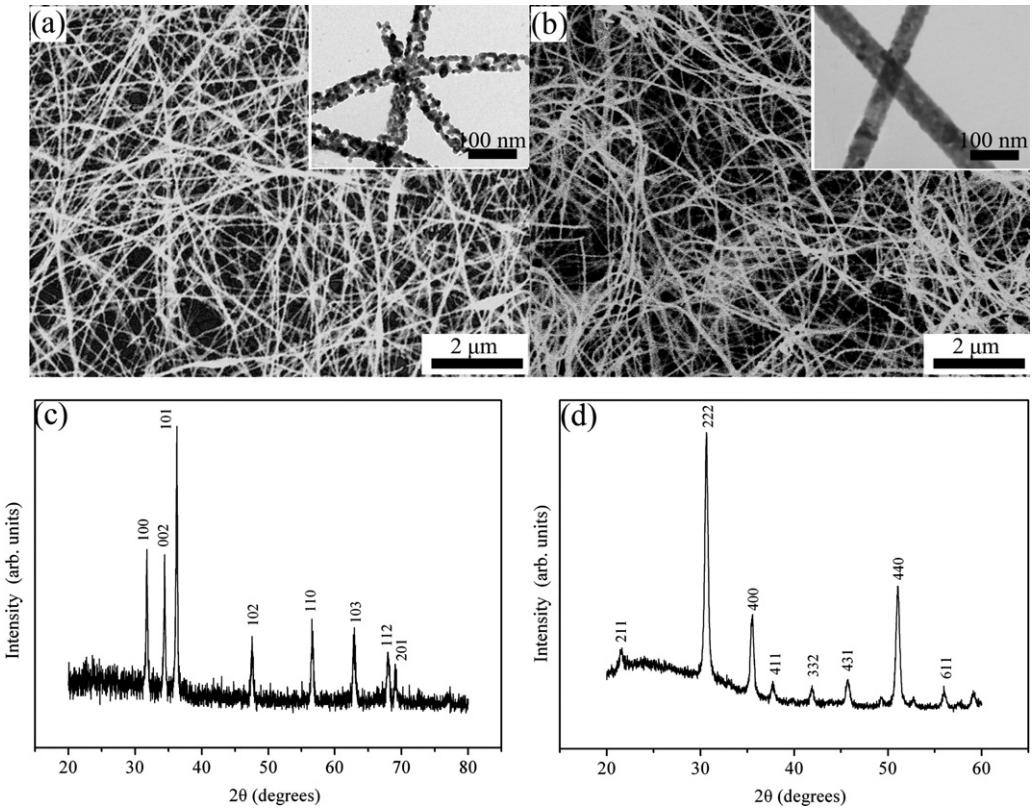

Fig. 3. SEM images of (a) ZnO and (b) In_2O_3 nanofibers (the inserts show corresponding TEM images), and XRD patterns of (c) ZnO and (d) In_2O_3 nanofibers.

in vacuum (<2 hPa) at 25 °C. Sample compositions and chemical states were confirmed by X-ray photoelectron spectroscopy (XPS, ESCALAB 250) with X-ray source (Al Kα $h\upsilon$ = 1486.6 eV). The binding energy in XPS spectra were calibrated with C 1s peak of 284.6 eV.

3. Results and discussion

Fig. 3(a) and (b) shows SEM images of ZnO nanofibers and In_2O_3 nanofibers, respectively. The two samples are highly dominated by the nanofibers with lengths of several ten micrometers and diameters ranging from 30 to 100 nm. Web-like micro-structure is naturally formed by nanofibers on the sensor substrates, and this structure is a benefit to the adsorption and desorption of gas molecules [22]. The TEM images inserted in Fig. 3(a) and (b) show that the nanofibers consisted of nanoparticles with an average diameter of about 10 nm. Fig. 3(c) and (d) display XRD patterns of ZnO nanofibers and In_2O_3 nanofibers, respectively. The diffraction peaks and their relative intensities match very well with those given by the JCPDS cards no. 36-1451 for hexagonal ZnO and no. 06-0416 for cubic In_2O_3.

Fig. 4(a) and (b) shows the FTIR spectra of ZnO nanofibers and In_2O_3 nanofibers, respectively. The main characteristic bands of ZnO are assigned as follows (Fig. 4(a)): The characteristic absorption peak at 3680 cm^{-1} is attributed to the presence of —OH group and the peaks around 2921, 2853, and 1514 cm^{-1} are corresponding to the stretching vibration of $—CH_3$, $—CH_2$, and C=C group, respectively. The peak at 1470 cm^{-1} may be the deformation vibration of C—H. The peak at 459 cm^{-1} may due to the intrinsic absorption of ZnO. For In_2O_3 nanofibers (Fig. 4(b)), the characteristic absorption peak at 3711 cm^{-1} should be attributed to the presence of —OH group and the peaks at 2966, 2899 and 1513 cm^{-1} are corresponding to the stretching vibration of $—CH_3$, $—CH_2$ and C=C group, respectively. The three sharp peaks at 601, 565 and 540 cm^{-1} may attribute to the phonon vibrations of In—O bonds [23].

Fig. 5(a) gives XPS survey type spectra of ZnO and In_2O_3, which shows the presence of Zn, In, O and adventitious C characteristic lines. Fig. 5(b) shows the O 1s XPS curves of ZnO and In_2O_3, which both can be consistently fitted by two nearly Gaussian, centered at 530.14 ± 0.01, 531.68 ± 0.02 eV, and 529.87 ± 0.03, 531.68 ± 0.02 eV, respectively. The components on the low binding energy side of the O 1s spectra in both of ZnO and In_2O_3 are attributed to the lattice oxygen. The one on the high binding energy side are attributed to the O^{2-} ions in the oxygen deficient regions within the matrix of ZnO and the medium state between O^{2-} and dissociated oxygen in In_2O_3, respectively [24–27].

In order to find the optimum conditions, the obtained films were exposed to 100 ppm ethanol at different temperatures and the sensitivity results are shown in Fig. 6(a). The ZnO nanofiber films show their highest sensitivity of 8 at 300 °C, which is similar as previous results [8]. After depositing In_2O_3 nanofibers, the obtained ZnO–In_2O_3 nanofiber films exhibit much higher sensitivity at a lower temperature. The sensitivity is enhanced to 25 at 210 °C. While ZnO–In_2O_3–ZnO films also exhibit low optimum temperature (210 °C), but the corresponding sensitivity decreases to 17. The above behaviors can be explained by the kinetics and mechanics of gas adsorption and desorption on the surface of semiconducting metal oxides. Normally, the sensor sensitivity is based on the cooperation of gas reactivity, oxygen state, base resistance (Ra), and the film structure (such as thickness). A high sensitivity can only be obtained at a suitable temperature with apropos sensing films [8,10]. Normally, the reactivity of the target gas with oxygen adsorbate is low, at low operating temperature, which leads to a very poor sensing response. When the temperature increased too much, the surface coverage of the oxygen adsorbate at the steadstate will be decreased, and that will limit the sensor performance eventually. Therefore, we could figure that ZnO–In_2O_3 nanofiber

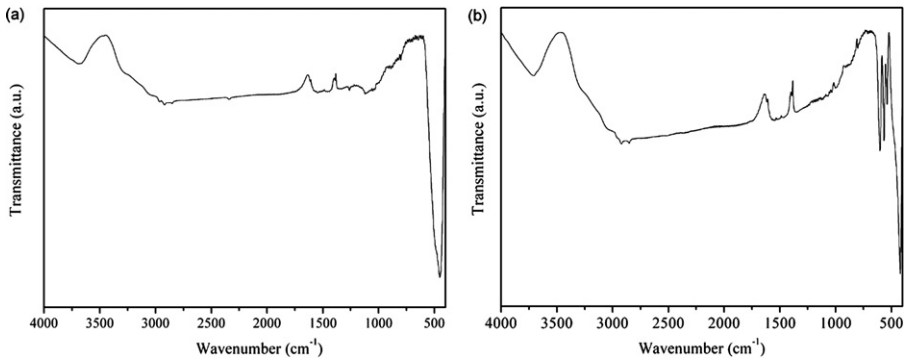

Fig. 4. Infrared absorption spectra of (a) ZnO and (b) In_2O_3 nanofibers.

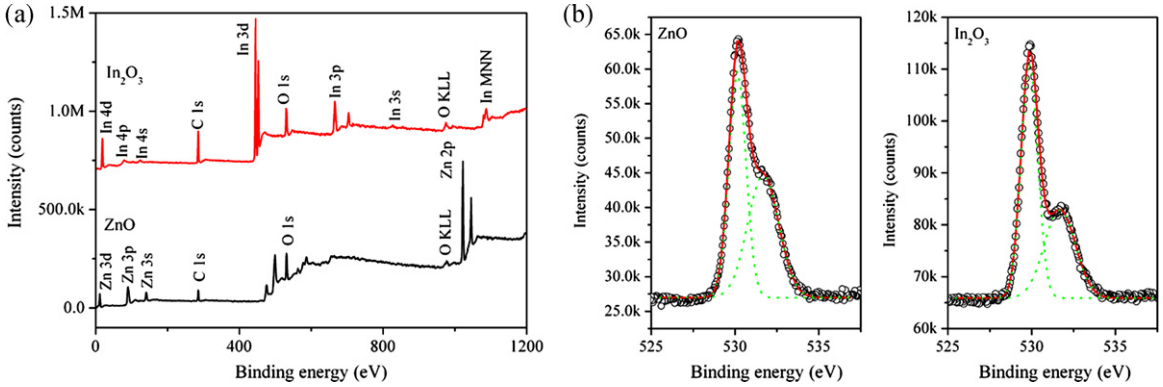

Fig. 5. (a) XPS survey spectra and (b) O 1s XPS curves of ZnO and In_2O_3 nanofibers.

films own the highest sensitivity and decreased operating temperature, thus all the studies hereinafter are focused on this type of films.

Fig. 6(b) shows the response-recovery characteristics of ZnO–In_2O_3 nanofiber films at 210 °C. The films exhibit rapid reaction speeds, and the response and recovery times are only 2 and 1 s to 100 ppm ethanol. When the films are exposed to 1000 ppm ethanol, the response and recovery times are increased to 6 and 2 s, respectively. This is mainly because longer reacting times are needed when the films meet higher concentration gas ambience (especially at low operating temperatures) [23].

Fig. 7 shows the film sensitivity versus ethanol concentration at 210 °C, and the insert is a calibration curve in the range of 1–500 ppm. The sensitivity rapidly increases by increasing ethanol concentration below 500 ppm. Above 500 ppm, the films become more or less saturated and the sensitivity slowly increases. Finally the films reach saturation at about 20,000 ppm. Good linearity is also found in the calibration curve, which further confirms that the present ZnO–In_2O_3 nanofiber films can be used as promising materials for ethanol detection.

The sensing mechanism of the presented films can be explained as follows [17]. Both ZnO and In_2O_3 are *n*-type semiconductors, and the oxygen vacancy in them acts as an electron donor to provide electrons to the conduction band. When the nanofiber films are surrounded by air, oxygen molecules will adsorb on the fiber surface to generate chemisorbed oxygen species (O_2^-, O^{2-}, or O^-), and O^- is believed to be dominant [17]. Consequently, depletion region will form on the fiber surface, resulting in a decrease of film conductibility. When the sensor is exposed to ethanol, ethanol molecules may react with O^- and release the trapped electron back to the conduction band, thus increasing the conductibility accordingly. The high performance of the ZnO–In_2O_3 nanofiber films is directly related to the fiber structure. The web-like structure of nanofiber films makes the absorption and desorption of gas molecules on the

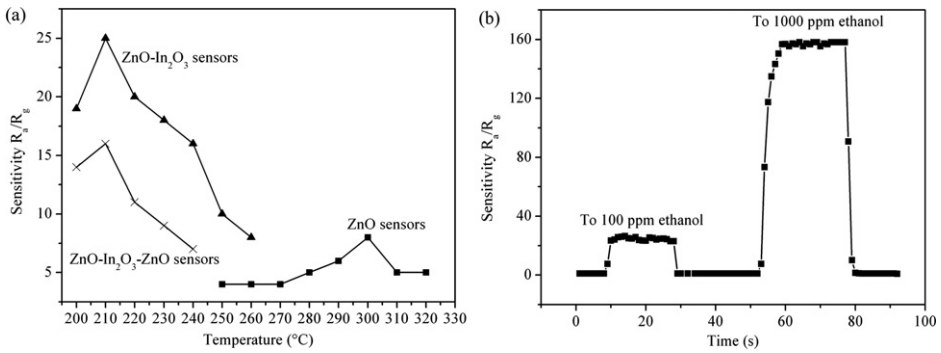

Fig. 6. (a) The operating temperature dependence of sensitivity for ZnO, ZnO–In_2O_3, and ZnO–In_2O_3–ZnO nanofiber films, and (b) response-recovery characteristic of ZnO–In_2O_3 nanofiber films to 100 and 1000 ppm ethanol at 210 °C.

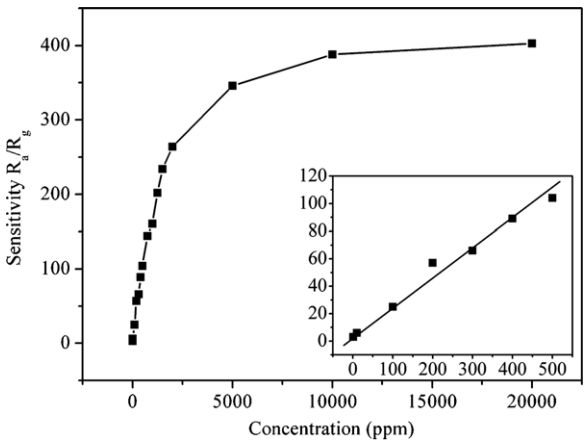

Fig. 7. Sensitivity of ZnO–In_2O_3 nanofiber films versus ethanol concentration. The insert shows a linear dependence of the sensitivity on ethanol concentration in the range of 1–500 ppm.

sensor surface easy [22]. And the 1D structures of the fibers can facilitate fast mass transfer of the ethanol molecules to and from the interaction region as well as improve the rate for charge carriers to transverse the barriers induced by molecular recognition along the fibers [12]. Additionally, taking the large surface to volume ratio, effective electron transport, and greatly reduced interfacial areas between the active sensing regions of the nanofibers, excellent ethanol sensing characteristics can be also found [28,29].

Compared with ZnO nanofiber films and ZnO–In_2O_3–ZnO nanofiber films, the ZnO–In_2O_3 nanofiber films exhibit much higher sensitivity at a low temperature. This can be explained by the nanofiber–nanofiber heterocontacts formed by the double-layer structure [30–33]. Such contacts will form a depleted layer around the intersection and thus block the electron flow in a way which is more efficient than the surface depletion of a single type of nanofibers [30,31]. The decreased sensitivity of ZnO–In_2O_3–ZnO nanofiber films can be explained by considering the film thickness. After depositing about 12 h, the higher film thickness may limit the signal transmission from film surface to electrodes [12], which leads to a decrease of film performance eventually.

4. Conclusions

In summary, ZnO and In_2O_3 nanofibers are synthesized through electrospinning methods and a double-layer sensing films are formed by spinning these nanofibers. Decreased optimum temperature, enhanced sensitivity and rapid response and recovery speeds are obtained based on the ZnO–In_2O_3 nanofiber films, and these properties are theoretically explained by considering the film structure. Our results suggest that ZnO–In_2O_3 nanofiber films are good candidates for ethanol detection, and the double-layer structure may be helpful in design high performance gas sensors.

Acknowledgments

The authors thank the National Natural Science Foundation of China (no. 50835007) for supporting this work.

References

[1] J. Janata, M. Josowicz, D.M. Devaney, Anal. Chem. 66 (1994) 207.
[2] J. Kong, N.R. Franklin, C. Zhou, M.G. Chapline, S. Peng, K. Cho, H. Dai, Science 287 (2000) 622.
[3] Y. Zeng, T. Zhang, H. Yang, L. Qiao, Q. Qi, F. Cao, Y. Zhang, R. Wang, Appl. Surf. Sci. 255 (2009) 4045.
[4] H.Y. Chen, S.P. Lau, L. Chen, J. Lin, C.H.A. Huan, K.L. Tan, J.S. Pan, Appl. Surf. Sci. 152 (1999) 193.
[5] X.Y. Xue, Y.J. Chen, Y.G. Wang, T.H. Wang, Appl. Phys. Lett. 86 (2005) 233101.
[6] H.A. Khorami, M. Keyanpour-Rad, M.R. Vaezi, Appl. Surf. Sci. 257 (2011) 7988.
[7] A. Aslani, V. Oroojpour, M. Fallahi, Appl. Surf. Sci. 257 (2011) 4056.
[8] Q. Qi, T. Zhang, X. Zheng, H. Fan, L. Liu, R. Wang, Y. Zeng, Sens. Actuators B 134 (2008) 36.
[9] J. Kaur, R. Kumar, M.C. Bhatnagar, Sens. Actuators B 126 (2007) 478.
[10] M.E. Franke, T.J. Koplin, U. Simon, Small 2 (2006) 36.
[11] Y.J. Chen, L. Nie, X.Y. Xue, Y.G. Wang, T.H. Wang, Appl. Phys. Lett. 88 (2006) 083105.
[12] A. Kolmakov, M. Moskovits, Annu. Rev. Mater. Res. 34 (2004) 151.
[13] Q. Kuang, C. Lao, Z.L. Wang, Z. Xie, L. Zheng, J. Am. Chem. Soc. 129 (2007) 6070.
[14] M. Davydova, A. Kromka, B. Rezek, O. Babchenko, M. Stuchlik, K. Hruska, Appl. Surf. Sci. 256 (2010) 5602.
[15] Y. Zhang, W. Fu, Y. Sui, H. Yang, J. Cao, M. Li, Y. Li, X. Zhou, Y. Leng, W. Zhao, H. Chen, L. Zhang, Q. Jing, H. Zhao, Appl. Surf. Sci. 257 (2011) 574.
[16] L.L. Xing, C.H. Ma, Z.H. Chen, X.Y. Xue, Appl. Surf. Sci. 257 (2011) 8576.
[17] N. Barsan, D. Koziej, U. Weimar, Sens. Actuators B 121 (2007) 18.
[18] L. Yu, X. Fan, L. Qi, L. Ma, W. Yan, Appl. Surf. Sci. 257 (2011) 3140.
[19] D. Li, Y. Xia, Adv. Mater. 16 (2004) 1151.
[20] Q. Qi, T. Zhang, S. Wang, X. Zheng, Sens. Actuators B 137 (2009) 649.
[21] B. Ding, M. Wang, X. Wang, J. Yu, C. Sun, Mater. Today 13 (2010) 16.
[22] Y. Zhang, J. Li, G. An, X. He, Sens. Actuators B 144 (2010) 43.
[23] S. Shukla, P. Zhang, H.J. Cho, S. Seal, L. Ludwig, Sens. Actuators B 120 (2007) 573.
[24] S.K. Poznyak, A.I. Kulak, Electrochim. Acta 45 (2000) 1595–1605.
[25] M. Chen, X. Wang, Y.H. Yu, Z.L. Pei, X.D. Bai, C. Sun, R.F. Huang, L.S. Wen, Appl. Surf. Sci. 158 (2000) 134–140.
[26] J.C. Lin, K.C. Peng, H.L. Liao, S.L. Lee, Thin Solid Films 516 (2008) 5349–5354.
[27] J.L. Huang, Y.T. Jah, B.S. Yau, C.Y. Chen, H.H. Lu, Thin Solid Films 370 (2000) 33.
[28] D. Zhang, Z. Liu, C. Li, T. Tang, X. Liu, S. Han, B. Lei, C. Zhou, Nano Lett. 4 (2004) 1919.
[29] M. Law, H. Kind, B. Messer, F. Kim, P. Yang, Angew. Chem. Int. Ed. 41 (2002) 2405.
[30] P. Feng, X.Y. Xue, Y.G. Liu, T.H. Wang, Appl. Phys. Lett. 89 (2006) 243414.
[31] P. Feng, Q. Wan, T.H. Wang, Appl. Phys. Lett. 87 (2005) 213111.
[32] Q. Qi, T. Zhang, L. Liu, X. Zheng, Sens. Actuators B 137 (2009) 471.
[33] A. Holzmeister, M. Rudisile, A. Greiner, J.H. Wendorff, Eur. Polym. J. 43 (2007) 4859.